Large eddy simulation of a collapsing vapor bubble containing non-condensable gas

Theresa Trummler*; Lukas Freytag; Steffen J. Schmidt and Nikolaus A. Adams

Chair of Aerodynamics and Fluid mechanics, Department of Mechanical Engineering, Technical University of Munich

Abstract

We investigate numerically the effect of non-condensable gas inside a vapor bubble on the bubble dynamics and the collapse pressure. Free gas in the vapor bubble has a cushioning effect that can weaken the pressure wave and enhance the bubble rebound. In order to access this effect numerically, simulations of collapsing vapor bubbles containing non-condensable gas are performed. In the simulations, the effects of the gas on the rebound and the shockwave energy are monitored for different operating points with varying initial gas contents $p_{g,0}$ inside the bubble and driving pressures Δp. For the cavitating liquid and the non-condensable gas we employ a homogeneous mixture model with a coupled equation of state for all components and the cavitation model is a barotropic thermodynamic equilibrium model, which is embedded in a higher order implicit large eddy approach for narrow stencils. Compressibility of all phases is considered, to capture the shockwave of the bubble collapse. The effect of the free gas on the rebound and the dampening of the emitted shockwave by the gas contained in the bubble are well captured by our simulations.

Keywords: bubble collapse; vapor bubble containing gas; energy partitioning; rebound; shock wave energy

Introduction

Liquids may contain dissolved gases that can be set free by pressure reduction or cavitation, leading to the presence of gas in vapor cavities. In experiments of bubble collapses the gas content in bubbles was shown to depend on whether they are generated using a laser or a spark and bubble dynamics were found to be influenced by this [1]. Gas inside the vapor bubble has a cushioning effect that can weaken the pressure wave and enhance bubble rebound. For spherical bubble collapses, this has already been investigated analytically and experimentally. However, for more complex configurations, the effect of the gas is not yet clarified and could be investigated with three-dimensional time resolved numerical simulations. Thus, the presented work serves as a validation of our modeling approach and a basis for later investigations.

In a vapor bubble containing free gas the pressure is $p = p_{\text{vap}} + p_{\text{g}}$, where p_{vap} denotes the vapor pressure and p_{g} the partial pressure of the gas. p_{g} depends on the compression of the bubble and assuming an adiabatic transformation of the gas it can be described with $p_{\text{g}}(t) = p_{\text{g},0} \cdot (R/R_0)^{1/\gamma}$. The index 0 indicates initial values and γ is the adiabatic index.

Tinguely et al. [2] experimentally and theoretically investigated the effects of the driving pressure difference $\Delta p = p_\infty - p_{\text{vap}}$ and the gas content $p_{\text{g},0}$ on bubble dynamics and shockwave emission. For their theoretical model they used an inviscid Keller Miksis model [3] taking advantage of the fact that it can be treated to first order [4]:

$$\rho((1-v)\ddot{R}R + 3/2\,\dot{R}^2(1-v)) = (1-v)(p_{\text{g}} - \Delta p) + R\dot{p}_{\text{g}}/c \tag{1}$$

with $v = \dot{R}/c$. Based on this model and their experimental measurements, they could show that the initial energy of a bubble $E_0 = \frac{4\pi}{3}R_0^3\Delta p$ [5] partitions mainly into rebound energy $E_{\text{reb}} = \frac{4\pi}{3}R_{\text{reb}}^3\Delta p$ and shockwave energy $E_{\text{SW}} = \frac{4\pi d^2}{\rho c}\int p(t)^2 dt$ [6]. In addition to this, they postulated that the energy partitioning between rebound ε_{reb} and shock wave energy ε_{sw} depends on a single parameter

$$\xi = \frac{\Delta p \gamma^6}{{p_{\text{g},0}}^{1/\gamma}(\rho c^2)^{1-1/\gamma}}, \tag{2}$$

where ρ, c are density and speed of sound in the liquid. The shockwave energy increases with ξ and thus with the driving pressure difference and decreases with the partial pressure of free gas. On the other hand, rebound is enhanced for a lower driving pressure difference and a higher gas content.

The aim of the presented work is to numerically investigate and reproduce the findings of Tinguely et al. [2] and to thereby validate our gas modeling approach.

*Corresponding Author, Theresa Trummler: *theresa.trummler@tum.de*

Thermodynamic model

We employ a multi-component homogeneous mixture model [7]. The cavitating liquid (lv) and the non-condensable gas (g) are described with one mixture fluid, which is defined by the volume averaged density inside a computational cell $\rho = \sum \beta_\phi \rho_\phi$. β_ϕ denotes the volume fraction and ρ_ϕ the density of each component $\phi = \{\text{lv},\ \text{g}\}$. This single fluid approach implies that within a computational cell all phases have the same velocity, temperature and pressure. Since the pressure in the bubble is $p = p_{\text{vap}} + p_{\text{g}}$, the pressure acting on the vapor is $p_{\text{vap}} = p - p_{\text{g}} = (1 - \beta_{\text{g}})\, p$. A coupled equation of state (EOS) gives the pressure as a function of the mean density $p = p(\rho)$ and is obtained by expressing the densities ρ_ϕ with the corresponding thermodynamic relations.

The cavitating water is described with a barotropic EOS, derived by integration of the isentropic speed of sound $\rho_{\text{lv}} = \rho_{\text{sat,liq}} + (p_{\text{lv}} - p_{\text{sat}})/c^2$, where $\rho_{\text{sat,liq}}$ is the saturation density for liquid water and p_{sat} the saturation pressure. Phase change is modeled assuming local thermodynamic equilibrium. For $p > p_{\text{sat}}$, there is purely liquid water and $c = 1482.35\,\text{m/s}$. For $p < p_{\text{sat}}$, there is a liquid vapor mixture with $c = 0.1\,\text{m/s}$ as a typical value for an equilibrium isentrop.

The non-condensible gas phase is described with $\rho_{\text{g}} = \rho_{\text{g,ref}} (p/p_{\text{ref}})^{1/\gamma}$, where $\rho_{\text{g,ref}}$ is the reference density at the reference pressure p_{ref}. In the presented results the gas is modeled isothermal with $\gamma = 1$.

Viscous effects are considered in our simulations using a linear blending with volume fractions for the mixture viscosity.

Numerical Method

The thermodynamic model is embedded in a density-based fully compressible flow solver. For the numerical model a higher order implicit large eddy approach for narrow stencils [8] is utilized. In implicit SGS the truncation error of the discretization serves as a subgrid-scale model for turbulence. Shockwaves and pseudo phase boundaries are detected with a sensor and in such regions an upwind based second order scheme is used. In smooth regions, on the other hand, a high order central discretization scheme with regularization terms is applied. Time integration is done using a 4-stage Runge-Kutta method with the Courant Friedrichs Lewy (CFL) number set to 1.4.

In [8], simulations of a spherical single vapor bubble collapse have been performed, comparing a more dissipative scheme and the applied one. The higher order discretization scheme was chosen for this work, since it resolves the pressure peaks more accurately.

Setup

A vapor bubble with an initial radius R_0 of $4 \cdot 10^{-4}$ m is placed in the center of a box with dimension $2\,L$ in each direction, where $L = 0.1$ m. Taking advantage of the symmetry, only an eighth of a vapor bubble is simulated. The domain is discretized with an equidistant grid within a cubic sub-domain with an edge length of $1.25\,R_0$ and for the outer part a grid stretching is applied. Simulations are performed on two different grids with 20 (coarse) and 80 (fine) computational cells over the initial bubble radius $1.25\,R_0$.

For the investigation, the initial gas content in the bubble $p_{\text{g,0}}$ and the driving pressure difference $\Delta p = p_\infty - p_{\text{sat}}$ are varied covering different combinations of $\Delta p = \{10\,\text{kPa}, 30\,\text{kPa}, 80\,\text{kPa}\}$ and $p_{\text{g,0}} = \{0\,\text{Pa},\ 100\,\text{Pa},\ 1000\,\text{Pa}\}$. During the simulations, the pressure signal is recorded by pressure probes placed in radial direction between $0.25\,R_0$ and $1.5\,R_0$ with a distance of $0.25\,R_0$.

Results

We mainly focus on the operating points $\Delta p = 10$ kPa with $p_{\text{g}} = 0$ Pa and $p_{\text{g}} = 100$ Pa and its ξ-equivalent $\Delta p = 100$ kPa; $p_{\text{g}} = 1000$ Pa. Fig. 1 (a) compares the temporal evolution of the normalized bubble radius R/R_0 for different gas contents and grid resolutions. The time is normalized to the Rayleigh collapse time $\tau_C = 0.915 \cdot R_0 \sqrt{\rho/\Delta p}$ [9]. Without gas, there is a very small rebound after the shockwave has propagated outwards. In configurations with gas the bubbles rebound significantly, and rebound increases with grid resolution, nearly matching the theoretical inviscid prediction of 42.7 % in maximum relative rebound radius

at 41% for the fine grid. Moreover, the results of the ξ-equivalent set-up on the coarse grid are shown and verify that there is a ξ - similarity for the rebound.

Besides the rebound, the non-condensable gas in the vapor bubble also affects the intensity of the emitted pressure wave. Fig. 1(b) shows the monitored pressure for the probes at different positions for different gas contents and grid resolutions. For all configurations, the radial decay of the maximum pressure is clearly visible and the presence of gas reduces the maximum pressure. The damping effect of the gas is, in general, more distinct for probes closer to the bubble center and stronger on the finer grid resolution. Additionally, the pressure signals reveal that the collapse time is perfectly matched. On the coarse grid the collapse time is slightly smaller, which is in agreement with the observations of [8]. The bubbles containing gas collapse later since the effective pressure difference is reduced by the gas.

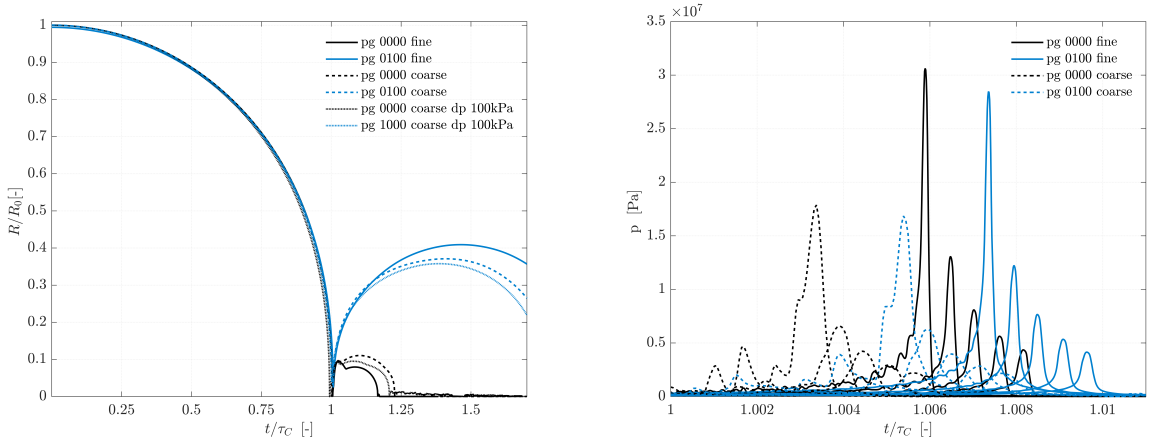

(a) Collapse dynamics of different configurations.

(b) Pressure signals from the probes $0.5\,R_0$-$1.5\,R_0$

Figure 1. Simulation results

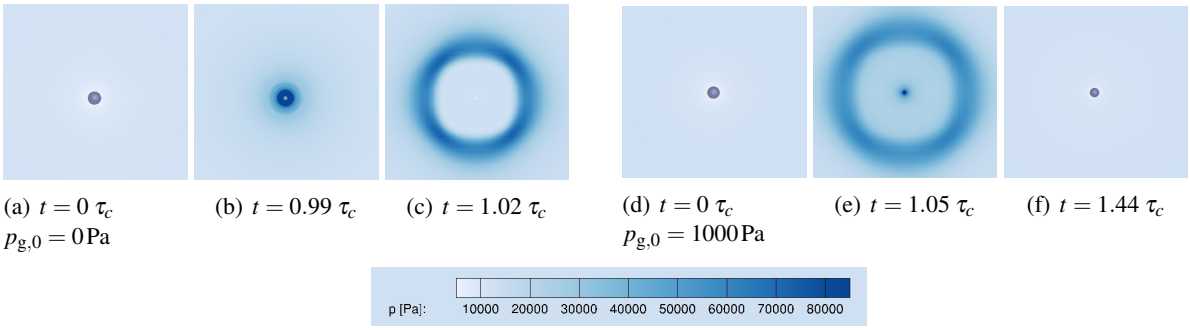

(a) $t = 0\ \tau_c$ $p_{g,0} = 0\,\text{Pa}$ (b) $t = 0.99\ \tau_c$ (c) $t = 1.02\ \tau_c$ (d) $t = 0\ \tau_c$ $p_{g,0} = 1000\,\text{Pa}$ (e) $t = 1.05\ \tau_c$ (f) $t = 1.44\ \tau_c$

Figure 2. Time series for $\Delta p = 10\text{kPa}$ with $p_{g,0} = 0$ and 1000Pa.

Fig. 2 depicts the bubble collapse and the rebound at different time steps for $\Delta p = 10\text{kPa}$ with $p_{g,0} = \{0\ \text{Pa}, 1000\ \text{Pa},\}$. The left time series presents the bubble collapse without gas, showing the initial bubble, the situation shortly before the collapse and the emitted shockwave after collapse. Analogously, the dynamics of a bubble with a high gas content is visualized in the right time series. In this case the rebound is clearly visible at $t = 1.44\ \tau_c$

In order to evaluate the energy partitioning, the normalized rebound energy ε_{reb} is obtained from the maximal radius of the bubble in the first rebound $\varepsilon_{\text{reb}} = (R_{\text{reb}}/R_0)^3$. For the normalized shockwave energy ε_{sw}, the pressure signals are numerically integrated and set in relation to the respective values without gas.

Fig. 3 compares the simulation results with the theoretical energy partitioning based on the solution of the adapted Keller-Miksis equation Eq. 1 over ξ. Our results are in good agreement with the theoretical ones and grid refinement leads to a better approximation to the theoretical model. Our simulation results confirm a ξ equivalence. The rebound for the ξ-equivalent configurations is the same, the normalized shockwave energy is higher for the higher pressure difference and better matches the theoretical model.

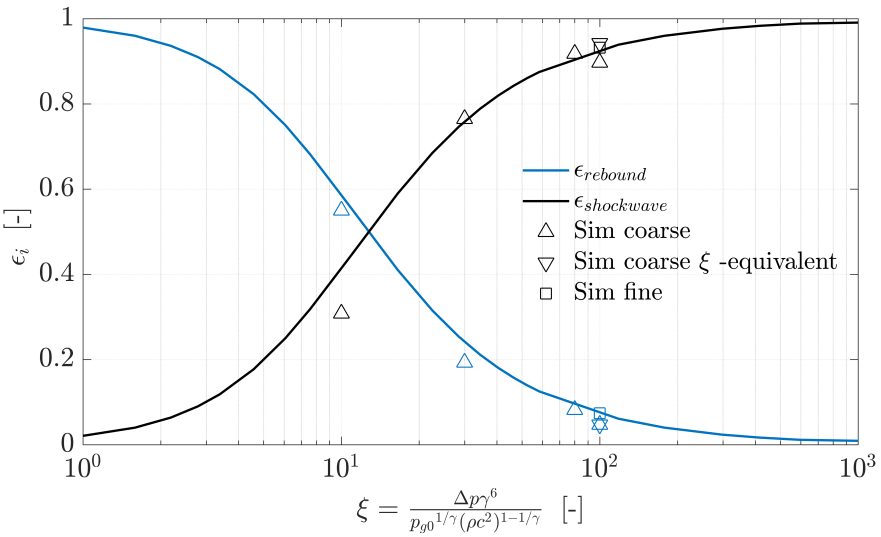

Figure 3. Simulation results in comparison with the theoretical energy partitioning proposed by Tinguely et al. [2].

Conclusion

With our simulations, we could reproduce the physical effects of gas inside a vapor bubble. Free gas in a vapor bubble leads to a stronger rebound and dampens the emitted shockwave. This effect is already visible on coarse grid resolutions, but gets more pronounced for higher grid resolutions. Additionally, we were able to reproduce the partitioning into rebound and shockwave energy proposed by Tinguely et al. [2] and could confirm a $\xi = (\Delta p \gamma^6)/({p_{g,0}}^{1/\gamma}(\rho c^2)^{1-1/\gamma})$ equivalence, i.e. same ξ-values result in the same rebound behavior and reduction of the shockwave energy. This validation allows us to investigate the effect of free gas on more complex configurations such as a bubble collapse at a wall.

References

[1] Sato T, Tinguely M, Oizumi M and Farhat M 2013 *Applied Physics Letters* **102** 074105–5
[2] Tinguely M, Obreschkow D, Kobel P, Dorsaz N, de Bosset A and Farhat M 2012 *Physical Review E* 1–7
[3] Keller J B and Miksis M 1980 *The Journal of the Acoustical Society of America* **68** 628–633
[4] Prosperetti A 1987 *Physics of Fluids* **30** 3626–4
[5] Obreschkow D, Kobel P, Dorsaz N, De Bosset A, Nicollier C and Farhat M 2006 *Physical review letters* **97** 094502
[6] Vogel A and Busch S 1996 *The Journal of the Acoustical Society of America* 1–18
[7] Örley F, Trummler T, Hickel S, Mihatsch M S, Schmidt S J and Adams N A 2015 *Physics of Fluids* **27** 086101–28
[8] Egerer C P, Schmidt S J, Hickel S and Adams N A 2016 *Journal of Computational Physics* **316** 453–469
[9] Rayleigh L 1917 *The London, Edinburgh, and Dublin Philosophical Magazine and Journal of Science* **34** 94–98